Taylor & Francis
Taylor & Francis Group

Chemical Engineering Communications

ISSN: (Print) (Online) Journal homepage: www.tandfonline.com/journals/gcec20

Synthesis of acrylic acid from methyl lactate over calcium phosphate catalysts in a fixed bed reactor: time-on-stream behavior and kinetic analysis

Atte Aho, Päivi Mäki-Arvela, Narendra Kumar, Ilari Angervo, Kari Eränen, Johan Wärnå, Tapio Salmi & Dmitry Yu Murzin

To cite this article: Atte Aho, Päivi Mäki-Arvela, Narendra Kumar, Ilari Angervo, Kari Eränen, Johan Wärnå, Tapio Salmi & Dmitry Yu Murzin (2024) Synthesis of acrylic acid from methyl lactate over calcium phosphate catalysts in a fixed bed reactor: time-on-stream behavior and kinetic analysis, Chemical Engineering Communications, 211:8, 1300-1318, DOI: 10.1080/00986445.2024.2338787

To link to this article: https://doi.org/10.1080/00986445.2024.2338787

Published online: 10 Apr 2024.

CHEMICAL ENGINEERING COMMUNICATIONS
2024, VOL. 211, NO. 8, 1300–1318
https://doi.org/10.1080/00986445.2024.2338787

Taylor & Francis
Taylor & Francis Group

RAPID COMMUNICATION

OPEN ACCESS Check for updates

Synthesis of acrylic acid from methyl lactate over calcium phosphate catalysts in a fixed bed reactor: time-on-stream behavior and kinetic analysis

Atte Aho[a], Päivi Mäki-Arvela[a], Narendra Kumar[a], Ilari Angervo[b], Kari Eränen[a], Johan Wärnå[a], Tapio Salmi[a], and Dmitry Yu Murzin[a]

[a]Laboratory of Industrial Chemistry and Reaction Engineering, Johan Gadolin Process Chemistry Centre, Åbo Akademi University, Åbo, Finland; [b]Wihuri Physical Laboratory, University of Turku, Turku, Finland

ABSTRACT

Transformation of methyl lactate to acrylic acid was investigated over $Ca_3(PO_4)_2$, $Ca_2(P_2O_7)$ and their mixture in the temperature range of 250-425 °C. The initial concentration of methyl lactate in water was varied from 2 wt% to neat methyl lactate. The results showed that these phosphate catalysts did not contain any measurable amounts of either acid sites or basic sites. The best catalyst was $Ca_3(PO_4)_2$ giving 62% selectivity to acrylic acid at 75% conversion at 400 °C using GHSV of 95280 h^{-1} and 2 wt% methyl lactate in the initial feed. This catalyst exhibited larger surface area in comparison to $Ca_2(P_2O_7)$. Elemental analysis revealed that some Ca leaching occurred during reaction, while in case of $Ca_2(P_2O_7)$ the calcium leaching was 3.4 fold higher than observed for $Ca_3(PO_4)_2$. Long-term results over $Ca_3(PO_4)_2$ showed that extensive catalyst deactivation occurred during the first 11 h time-on-stream, after which the activity dropped only slightly. In addition to kinetic studies with different parameters, also, kinetic modeling was performed and the activation energies for formation of different products were determined over different catalysts.

KEYWORDS

Acrylic acid; calcium phosphate; kinetic modeling; methyl lactate

Introduction

Acrylic acid and its esters, acrylates, have a wide application range as monomers for the eventual production of paints, coatings, adhesives, super-absorbent etc. (Murphy et al. 2018). Currently, acrylic acid is mainly produced through selective oxidation of fossil propylene (Zhang et al. 2016). In a two-step process propylene is oxidized in the first step to propenal followed by its oxidation to acrylic acid giving ca. 90% of the overall yield (Tichý 1997). The idea to produce bioacrylic acid from renewable resources has attained a lot of interest in the recent years (Holmen 1958; Walkup et al. 1993; Tam et al. 1997; Shi et al. 2007; Wang et al. 2008; Zhang et al. 2008; Lee et al. 2010; Sun et al. 2010, 2009, 2011, 2014; Hong et al. 2011, 2014, 2020, 2009; Blanco et al. 2014; Ghantani et al. 2014, 2013; Li et al. 2014; Peng et al. 2014; Tang et al. 2014a, 2014b; Yan et al. 2014a, 2014b, 2011; Näfe et al. 2015; Yuan et al. 2015; Lari et al. 2016; Murphy et al. 2016a, 2016b, 2017; Liu et al. 2020;Nekkala et al. 2022; Sobuś and Czekaj 2022; Dhiman et al. 2023). Different biomass derived feedstock has been applied as a raw material to synthesize bioacrylic acid, such as lactic acid (Holmen 1958; Walkup et al. 1993; Tam et al. 1997; Wang et al. 2008; Sun et al. 2010, 2009; Blanco et al. 2014; Ghantani et al. 2014, 2013; Peng et al. 2014; Zhang et al. 2014, 2011; Tang et al. 2014a, 2014b; Näfe et al. 2015; Yuan et al. 2015; Lari et al. 2016; Yan et al. 2020, 2014a, 2014b, 2011; Nekkala et al. 2022; Sobuś and Czekaj 2022; Dhiman et al. 2023) and alkyl lactates (Shi et al. 2007; Zhang et al. 2008, 2009; Lee et al. 2010; Hong et al. 2011; Li et al. 2014; Wang et al. 2014; Murphy et al. 2017, 2016a, 2016b; Liu et al. 2020), glycerol (Talebian-Kiakalaieh et al. 2014), fumaric acid (Burk et al. 2011) and 3-hydroxypropionic

CONTACT Dmitry Yu Murzin dmurzin@abo.fi Laboratory of Industrial Chemistry and Reaction Engineering, Johan Gadolin Process Chemistry Centre, Åbo Akademi University, Åbo, Finland.

acid (Craciun et al. 2009). The latter can be produced by fermentation of sugars (Jiang et al. 2009) with fumaric acid also present in the fermentation broth (Burk et al. 2011). Recently, processes to generate 3-hydroxypropionic acid and further transform it to acrylic acid have been developed by several companies, including BASF, Dow Chemical, Cargill and Novozymes (Rodrigues 2022). Lactic acid, which can be formed from sugars over heterogeneous catalysts (Mäki-Arvela et al. 2020) or by fermentation of biomass (Datta and Henry 2006) has been intensively used as a feedstock for synthesis of acrolein. The drawback in using fermentation for lactic acid synthesis is the high boiling point and chemical instability of lactic acid requiring its conversion into metal salts before separation and purification from the fermentation broth (Datta and Henry 2006). One of the initial reports for dehydration of lactic acid to acrylic acid goes back all the way to 1950s (Holmen 1958) using Na_2SO_4 and $CaSO_4$ as catalysts. Superficially, the reactions taking place during dehydration of methyl lactate to either acrylic acid or methyl acrylate are fairly simple with only one major side reaction forming acetaldehyde, carbon monoxide and methanol as shown in Scheme 1. Possible de-esterification of the methyl acrylate to acrylic acid can occur if the reactions are carried out in the presence of water.

Several types of catalysts have been used in transformations of methyl lactate to acrylic acid including alkali metal cation exchanged zeolites (Murphy et al. 2018; Yan et al. 2020) as well as sodium and calcium phosphates (Zhang et al. 2009; Lee et al. 2010; Hong et al. 2011). High acrylic acid yields were obtained with calcium phosphates, such as $Ca_3(PO_4)_2$-SiO_2 (Lee et al. 2010) and $Ca_3(PO_4)_2$-$Ca_2(P_2O_7)$ composite catalyst (Hong et al. 2011). In the former case, the combined selectivity to acrylic and methyl acrylate was 77% at 74% conversion (Lee et al. 2010). The same activity was retained for 100 h continuous reaction giving the final selectivity to acrylic acid and methyl lactate of also 77%. In the case of $Ca_3(PO_4)_2$-$Ca_2(P_2O_7)$ at 91% conversion selectivity to acrylic acid and methyl lactate was 75% and 5%, respectively (Hong et al. 2011). The desired catalyst properties were reported to be of moderate acid-base strengths. However, the catalytic data (Lee et al. 2010; Hong et al. 2011) with calcium phosphates as catalysts are rather limited as neither gas phase analysis nor carbon balances were reported.

The aim in this work was to synthesize, characterize and test $Ca_3(PO_4)_2$ and $Ca_2P_2O_7$ catalysts in transformations of methyl lactate to acrylic acid. The main parameters were the initial concentration of methyl lactate, temperature, the gas and liquid flow rates. Furthermore, the time-on-stream behavior, the carbon balance and the gas phase composition will be reported and the catalyst performance will be correlated with their properties. In addition, kinetic modeling was performed.

Experimental

Chemicals

The chemicals used in the work are listed below: methyl lactate (Aldrich, 98%), acrylic acid (Aldrich, 99%), acetaldehyde (Fluka, ≥99.5%), methanol (Sigma-Aldrich, ≥99.9%), methyl acrylate (Alfa Aesar, 99%), $Na_3PO_4{\cdot}12H_2O$ (Sigma-Aldrich, ≥98%), $Na_4P_2O_7$ (Sigma-Aldrich, ≥95%), $CaCl_2{\cdot}2H_2O$ (Sigma-Aldrich, ≥99%), argon (Woikoski, N50), CO/CO_2 calibration gas (Woikoski, 1%, 1%), pyridine, (Acros Organics, 99%) and ion-exchanged water (ELGA, Purelab Chorus, 18.2 MΩ.cm).

Catalyst synthesis

Calcium phosphate synthesis

Calcium phosphate was prepared according to the procedure reported by Hong et al. (Hong et al. 2011). The preparation was carried out by precipitating a 250 mL solution of 0.4 M $Na_3PO_4{\cdot}12H_2O$ with a slow addition of 100 mL 1.6 M $CaCl_2{\cdot}2H_2O$ solution at 60 °C. After precipitation, the solid material was recovered through filtration, washed twice through re-dispersion in ion-exchanged water with filtration between the washing steps, dried at 80 °C overnight and finally heated to 500 °C for 6 h.

Calcium pyrophosphate synthesis

Calcium pyrophosphate $Ca_2P_2O_7$ was prepared according to the procedure reported by Hong et al. (Hong et al. 2011) with some modifications. The preparation was carried out by precipitating

a 250 mL solution of 0.488 M $Na_4P_2O_7$ with a slow addition of 100 mL 2.68 M $CaCl_2{\cdot}2H_2O$ solution at 60 °C. While Hong et al. (Hong et al. 2011) carried out precipitation at the room temperature, at room temperature solubility of $Na_2P_2O_7$ in water is very limited and therefore, the synthesis was carried out at 60 °C. After precipitation, the solid material was recovered through filtration, washed twice through re-dispersion in ion-exchanged water with filtration between the washing steps, dried at 80 °C overnight and finally heated to 500 °C for 6 h.

Preparation of composite material

The composite $Ca_3(PO_4)_2$ + $Ca_2P_2O_7$ materials was prepared through dispersion of equal parts of the calcium materials, described above, in 350 mL ion-exchanged water, filtered, washed and dried at 80 °C and finally thermally treated at 500 °C for 6 h.

Catalyst characterization

XRD

The X-ray diffraction (XRD) characterization was performed using PANalytical Empyrean diffractometer with five axis goniometer. An Empyrean Cu LFF X-ray tube was used and the X-ray radiation was filtered to include only components of Cu $K_{\alpha1}$ and Cu $K_{\alpha2}$. The results were analyzed with MAUD (Material Analysis Using Diffaction) analysis program. Instrumental broadening was evaluated with the Si standard sample. The results were obtained with 2θ scan range from 5° to 120°.

SEM-EDX

A Leo Gemini 1530 microscope, Scanning Electron Microscopy (SEM), was used to study the crystal morphology, shape and size of the catalysts. The elemental compositions of the catalysts were analyzed by Energy-dispersive X-ray spectroscopy (EDX) coupled to SEM.

TEM

The catalysts were investigated by Transmission Electron Microscopy (TEM) using a JEOL JEM-1400 Plus microscopy equipped with a bottom mounted OSIS Quemesa digital camera.

N_2-physisorption

The specific surface area of the catalysts was measured with a Micrometrics MicroActive 3Flex 3500. Prior to the surface area measurements, the catalyst samples were outgassed at 250 °C for 4 h.

Pyridine-FTIR

Pyridine was used as a probe molecule to determine the acidity, its strength and type of acid sites by Fourier Transformed Infrared Spectroscopy (FTIR), (ATI Mattson FTIR). The catalysts were pressed into thin disks and placed in a cell. Prior to pyridine adsorption at 100 °C (30 min) the cell was outgassed at 450 °C for 1 h followed by desorption at 250 °C, 350 °C and 450 °C. The spectra were recorded at 100 °C in between every desorption temperature. Spectral bands at 1545 cm^{-1} and 1450 cm^{-1} were used to identify Brønsted (BAS) and Lewis acid sites (LAS), respectively.

Ammonia TPD

Temperature programmed desorption of ammonia (NH_3-TPD) was performed using Microtrac Belcat II equipment equipped with a thermal conductivity detector. The catalyst sample (ca. 50 mg) was pretreated at 300 °C for 1 h. Thereafter, the sample was cooled to 100 °C, ammonia (5% in He, 30 mL/min) was adsorbed at 100 °C for 30 min to the catalyst, followed by flushing with 30 mL/min of helium at the same 100 °C for 1 h before finally decreasing the temperature to 50 °C. The desorption of NH_3 was monitored with the TCD as the temperature was increased from 50 to 600 °C with a heating rate of 10 °C/min, after reaching the final temperature it was kept isothermal for 20 min. The response of the TCD was calibrated by analyzing known concentrations of NH_3 in helium to quantify the amount of desorbed ammonia.

CO_2-TPD

Basicity was determined by temperature programmed desorption (TPD) of CO2 using a Microtrac MRB, Belcat II device. The catalyst sample was dried in the sample tube prior to adsorption of CO2 at 400 °C for 30 min. Adsorption of CO2 was carried out at 100 °C for 30 min with a 20 mL/min flow. The TPD of CO2 was performed with a heating rate of 10 °C/min from 100 °C to 600 °C, the desorbed CO2 was flushed away from

the sample tube with a 20 mL/min flow of helium and analyzed with an OmniStar mass spectrometer.

Reactor set-up and experimental procedure

The reactor set-up consisted of a quartz reactor tube ($L = 40$ cm, I.D. 9.4 mm) heated by a Carbolite (MTF 12/25/250) furnace. The reactor tube was placed in aluminum blocks to improve the heat transfer from the furnace to the reactor tube. A K-type thermocouple was used to monitor and control the temperature of the furnace, the tip of the thermocouple was placed in a way that it was at the same height as the catalyst in the reactor tube. An Eldex pump pushed the methyl lactate solution to the reactor. The reactant bottle was placed on a Precisa 12400 DG-FRSCS balance to quantify the feeding rate. Argon was used to flush the gaseous methyl lactate – water vapor through the reactor with the argon flow controlled with a Brooks Mass Flow Controller (5850 E Series). Both the gas and liquid flows entered from the top of the reactor tube. Downstream the reactor a spiral cooler of the size 35×3 cm was applied to condense the liquid products at 0.5 °C with a LAUDA Ecoline RE106. The liquid products were collected in a 25 mL 3-neck bottle and the samples were withdrawn periodically from it. The uncondensed gases were passed to a Siemens Ultramat 6 CO/CO_2 analyzer.

In a typical experiment, the reactor was filled by plugging the bottom part of the reactor tube with quartz wool to prevent that the reactor content could come out. Then 15 g of (3 mm) glass beads were loaded to the reactor placing them thus at the bottom. Thereafter a thin layer of quartz wool was placed above the glass beads, followed by 0.5 g of quartz sand (250-355 µm), 50 mg of the catalyst (125-250 µm), 0.5 g of quartz sand, 5 g of glass beads and finally 5 g of quartz sand to fill the remaining part of the reactor tube. Thin layers of quartz wool were placed between every type of the reactor content to avoid mixing of them and allow easy separation after the experiments.

After the reactor was filled, it was placed inside the aluminum block and subsequently inside the furnace, secured to the inlet and leak-tested. Thereafter, heating of the furnace was started with a 5 °C/min heating rate. When the desired reaction temperature was reached, typically starting at 250 °C, pumping of the methyl lactate solution was commenced along with the data logging for gas concentrations. The liquid samples were withdrawn for analysis every hour by first removal of the waste samples 30 min prior to sampling. The temperature program used for catalyst screening was 1 h at 250-375 with 25 °C increments. The reactor operated under atmospheric pressure.

Product analysis

The concentrations of CO and CO_2 were analyzed with a Siemens Ultramat 6 gas analyzer. The analyzer was calibrated with a calibration gas containing 1% of both CO and CO_2. The liquid products and the reactant solution were analyzed with a Hewlett Packard (HP 6890 Series) gas chromatograph equipped with a flame ionization detector (FID). The column used for separation of the reactant and products was an Agilent Technologies DB-FFAP 60 m x 0.250 mm, 0.25 Micron. The temperature program used in the GC-analysis was as follows: starting at 50 °C with 2 min hold, heating to 220 °C with 10 °C/min and then holding for 10 min hold. Quantification of the detected compounds was done by using the FID response factor obtained through analyzing known concentrations of methyl lactate, acrylic acid, acetaldehyde, methanol and methyl acrylate. Note, that the boiling point of acetaldehyde is 20.2 °C. Therefore, preparation of acetaldehyde standard solutions was made in chilled volumetric flasks and diluted with cold ion-exchanged water. Moreover, it is possible that a certain amount of acetaldehyde is not condensed and collected in the cooler used in the reactor set-up.

Calculations

Conventional expressions for conversion, selectivity and yield have been used. Methyl lactate conversion was calculated from

$$X = \frac{c_0 - c_i}{c_0} \quad (1)$$

where c_0 indicates the concentration in the feed and c_i the concentration in a reaction mixture sample.

Selectivity was calculated with the following equation:

$$S = \frac{c_{p,i}}{c_0 - c_I} \quad (2)$$

The space time yield (STY) was related to the unit of time and catalyst mass:

$$STY = \frac{\dot{n}_{AA}}{m_{cat}} \quad (3)$$

Where $\dot{n}_{AA}$ is the molar flow of acrylic acid in the reaction mixture sample and m_{cat} catalyst mass. No stoichiometric factors were applied in the calculations since all products are formed in 1:1 ratio to methyl lactate as shown in Scheme 1.

The carbon balance (CB) was calculated with Equation (4) taking into account reactions stoichiometry:

$$X_{CB} = \frac{4c_i + 3c_{AA,i} + c_{MeOH,i} + 3c_{CO,i} + c_{CO2,i}}{4c_0} \quad (4)$$

where $c_{AA,I}$ is the concentration of acrylic acid, $c_{MeOH,I}$ concentration of methanol, c_{CO},i and $c_{CO2,i}$ concentrations of carbon monoxide and carbon dioxide. The coefficients before the concentrations indicate the number of carbon atoms

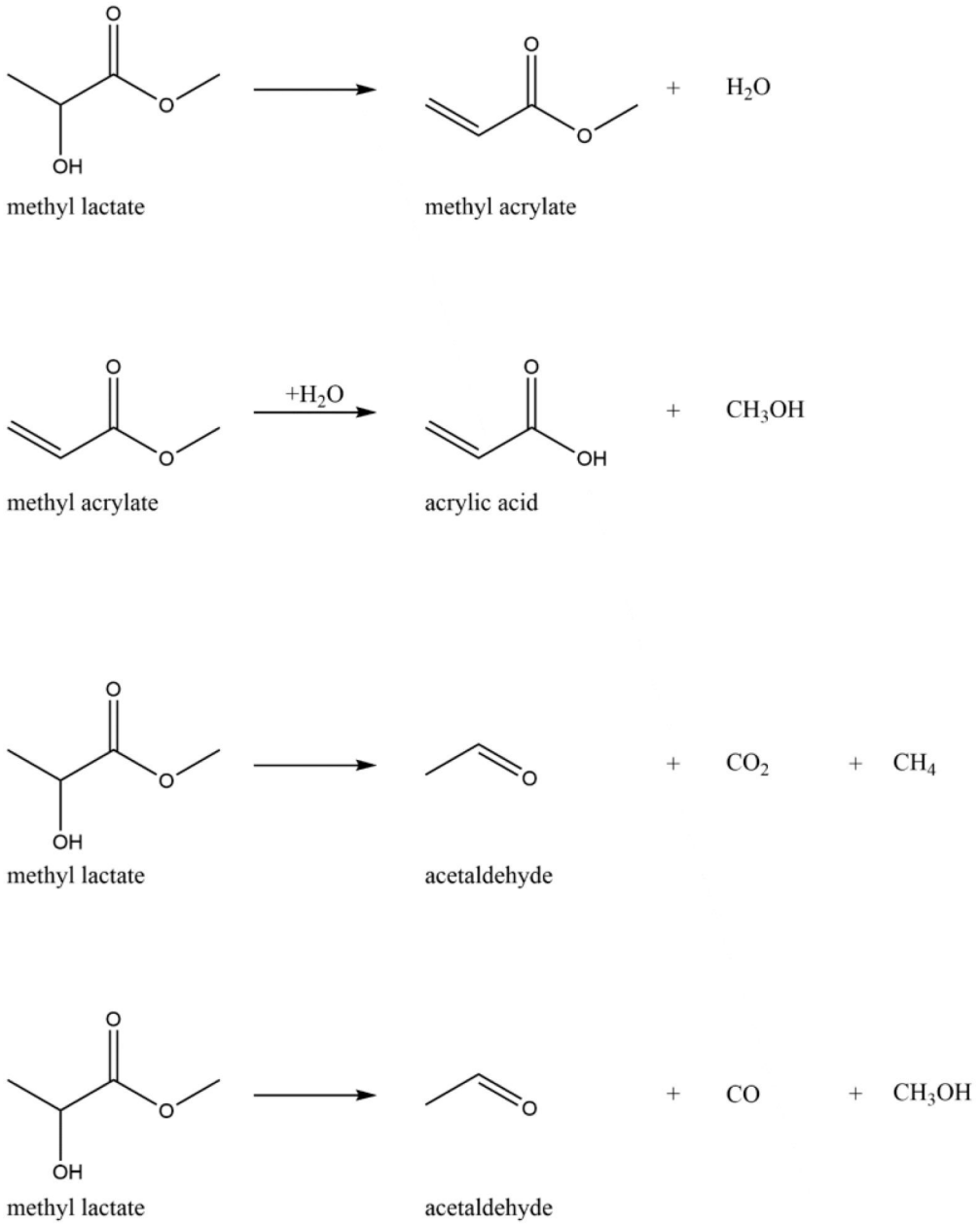

Scheme 1. A Reaction scheme for dehydration of methyl lactate to acrylic acid and methyl acrylate as well as the main parallel side reactions to acetaldehyde.

in each compound, except for $c_{CO,I}$ where it originates from the sum of carbon atoms in CO and acetaldehyde. The reason for not using the concentration of acetaldehyde obtained with GC analysis is a probability that not all acetaldehyde is collected in the cooler, as explained above, and therefore a more precise carbon balance could be obtained by using the concentration of CO instead of acetaldehyde.

Results and discussion

Catalyst characterization results

TEM results

The calcium-phosphate catalysts were investigated by TEM, shown in Figure 1. Calcium phosphate particles of the diameter in the range of 40 nm to 60 nm have a round shape or partially elongated shapes. At this magnification calcium pyrophosphate structure is rather similar to the structure of calcium phosphate.

SEM-EDX results

Two different calcium-phosphate catalysts were also investigated by SEM-EDX with the micrographs shown in Figure 2. The surface morphology differs significantly between the two calcium-phosphate catalysts. The surface of the $Ca_3(PO_4)_2$ catalyst (Figure 2a) is fairly uniform with significant surface roughness, while the $Ca_2P_2O_7$ catalyst (Figure 2b) exhibits both rough and smoother areas. The samples were prepared through precipitation of sodium phosphates with $CaCl_2$, thus presence of sodium could be anticipated. The sodium content of the catalysts was determined by SEM-EDX being 1.1% and 10.2% for $Ca_3(PO_4)$ and $Ca_2P_2O_7$ catalysts, respectively. A reason for the high sodium content in the latter is probably due to a low solubility of $Na_4P_2O_7$, as reported above in the section on preparation of this material.

The elemental analysis of the spent $Ca_2P_2O_7$ and $Ca_3(PO_4)_3$ is also reported in Table 1. The results showed that the Ca/P ratio for the fresh and spent $Ca_2P_2O_7$ decreased from 1.1 to 0.9, while the corresponding values for $Ca_3(PO_4)_3$ were 2.2 and 2.1, respectively. These values demonstrate that the Ca/P ratio decreased for the former one by 17%, while for $Ca_3(PO_4)_3$ the Ca/P ratio decreased only by 5%.

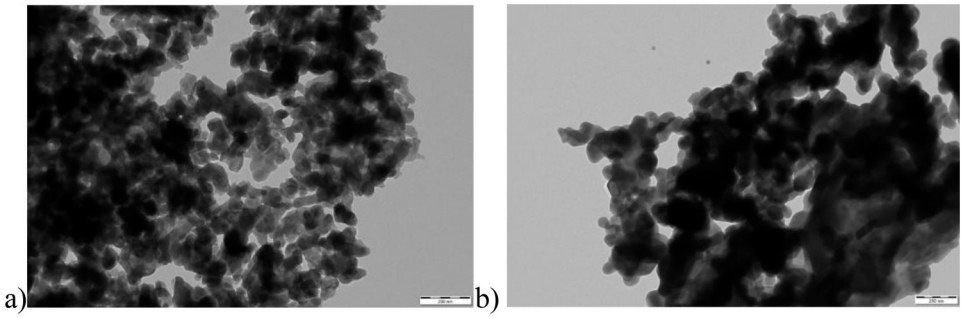

Figure 1. TEM images of (a) $Ca_3(PO_4)_2$ and (b) $Ca_2(P_2O_7)$ catalysts.

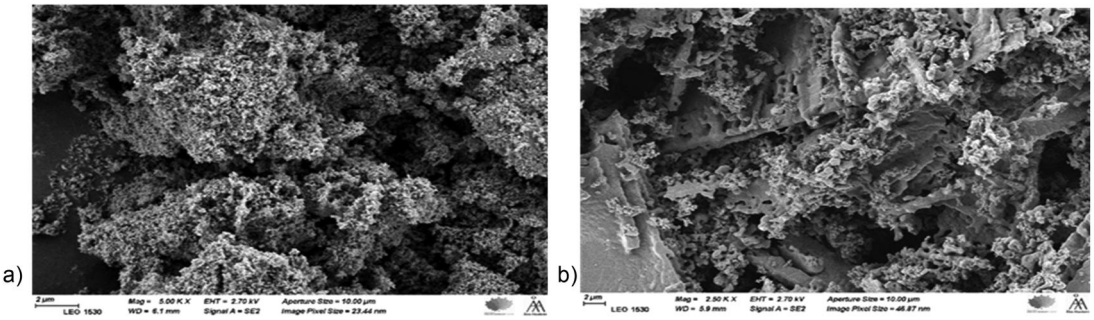

Figure 2. SEM images of (a) $Ca_3(PO_4)_2$ and (b) $Ca_2P_2O_7$ catalysts.

Table 1. Elemental analysis of $Ca_2P_2O_7$ and $Ca_3(PO_4)_2$ catalysts.

Element	$Ca_2P_2O_7$ wt%	$Ca_2P_2O_7$ spent wt%	$Ca_2P_2O_{7theor.}$ wt%	$Ca_3(PO_4)_2$ wt%	$Ca_3(PO_4)_2$ spent wt%	$Ca_3(PO_4)_{2,theor.}$ wt%
O	41.9	45.75±0.36	44.08	49.19±0.25	44.52±0.46	41.27
Na	11.46±0.11	15.12±0.13	0	1.17±0.06	1.11±0.08	0
P	21.96±0.11	18.36±0.12	24.38	15.41±0.11	16.49±0.11	19.27
Cl	0.72±0.04	0.31±0.05	0	0.40±0.03	0.31±0.05	0
Ca	23.96±0.12	16.68±0.14	31.55	33.75±0.19	33.97±0.20	38.76
Si	0	0	0	0.07±0.03	0.09±0.03	0

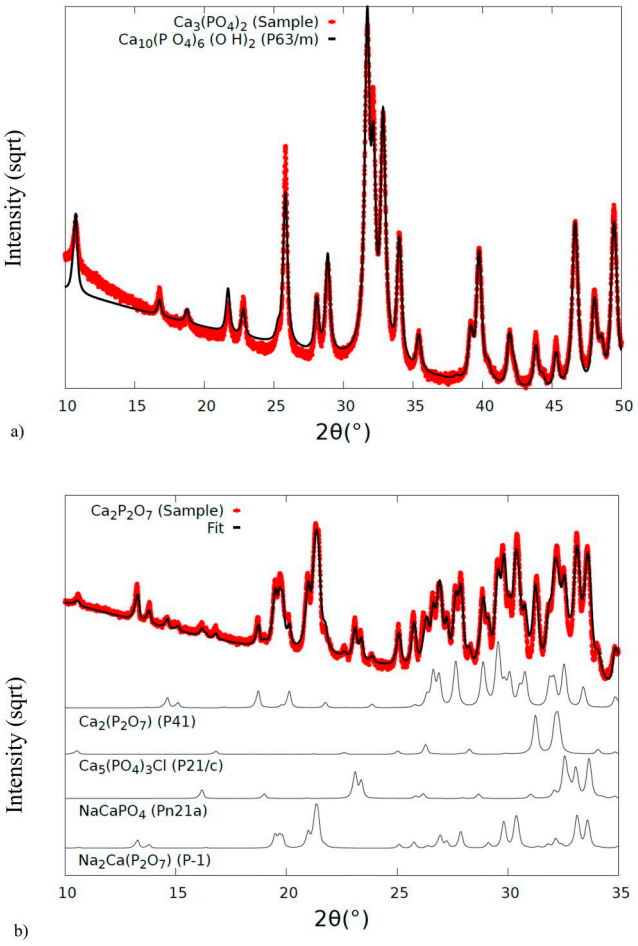

Figure 3. Diffractograms of (a) $Ca_3(PO_4)_2$, (b) $Ca_2P_2O_7$ with fitted standardized diffraction patterns.

XRD-results

The XRD results for the fresh $Ca_3(PO_4)_2$ and $Ca_2P_2O_7$ are shown in Figure 3. XRD pattern of the fresh $Ca_3(PO_4)_2$ can be explained with the presence of a single phase of $Ca_{10}(PO_4)_6(OH)_2$ (Ardanova et al. 2010) (space group P63/m). A fitted model of the diffraction pattern is presented in Figure 3a. Figure 3b diffraction results for the fresh $Ca_2P_2O_7$ with various phase candidates. A reasonable match with the diffraction results and the model was obtained with the combination of four fitted phase candidates including $Ca_2P_2O_7$ (Boudin et al. 1993), $Ca_5(PO_4)_3Cl$ [ICDD PDF 04-023-5241], $NaCa(PO_4)$ (Ben Amara et al. 1983) and $Na_2Ca(P_2O_7)$ (Bennazha et al. 1999).

Table 2. Nitrogen physisorption results for some of the tested catalysts.

Catalyst	A (m^2/g)	V (cm^3/g)	r (nm)
$Ca_3(PO_4)_2$	16 (11)[a]	0.01	0.995
$Ca_2P_2O_7$	<1		

[a]in parenthesis for the spent catalyst.

N_2-physisorption results

The specific surface area, the pore volume and the pore radius were measured for some selected catalysts as listed in Table 2. For both materials, these surface areas are lower than those reported in Hong et al. (2011). One reason for the lower surface area of calcium pyrophosphate could be its high sodium content. Specific surface area of the spent $Ca_3(PO_4)_2$ was 31% lower than that for the fresh one which is apparently related to catalyst deactivation.

Pyridine-FTIR, ammonia TPD and CO_2 TPD results

No meaningful acidity could be determined by FTIR of pyridine being at the background level. However, when the acidity of both catalysts was determined by ammonia TPD the results showed that $Ca_3(PO_4)_2$ exhibited more than 11 fold higher acidity than $Ca_2P_2O_7$ (Figure 4). The specific acidity of the materials is 485 µmol/g and 43 µmol/g for the $Ca_3(PO_4)_2$ and $Ca_2P_2O_7$, respectively. This result is in accordance with the trend reported by Hong et al. (2011), with acidity of $Ca_3(PO_4)_2$ being ca. 2 fold higher than for $Ca_2P_2O_7$.

No CO_2 signal could be detected with the MS indicating absence of basic sites that could adsorb CO_2.

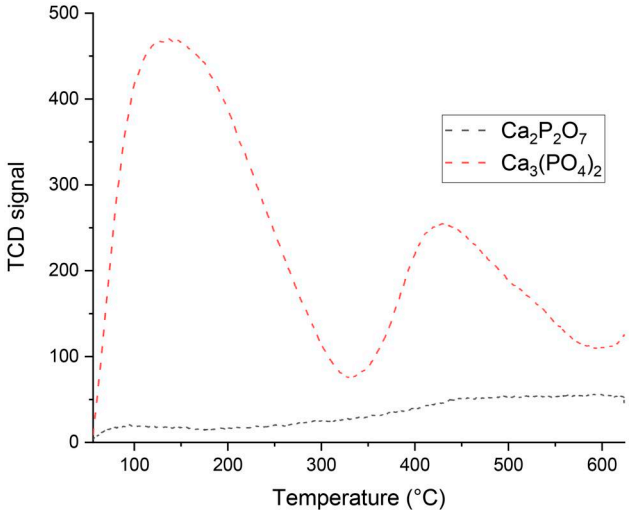

Figure 4. Ammonia TPD results for $Ca_3(PO_4)_2$ and $Ca_2(P_2O_7)$.

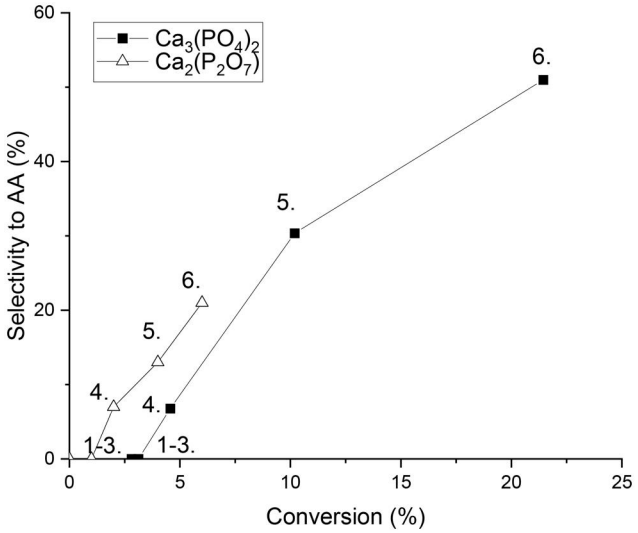

Figure 5. Selectivity as a function of conversion in methyl lactate transformation to acrylic acid (AA). Notation: 1. 250 °C, 2. 275 °C, 3. 300 °C, 4. 325 °C, 5. 350 °C, 6. 375 °C. Conditions: GHSV = 95280 h^{-1}, contact time 30 s, catalyst mass 50 mg.

Catalytic results

Activity and temperature dependence

Prior to catalytic tests a blank run was performed without any catalyst, resulting in a very low methyl lactate conversion. Two different phosphates were investigated in synthesis of acrylic acid from methyl lactate, namely calcium phosphate $Ca_3(PO_4)_2$ and calcium pyrophosphate $Ca_2P_2O_7$ as well as their mixture. It was observed, that these catalysts were not very active in the temperature range of 250 – 375 °C, when the experiments were performed at a specific temperature for 1 h and then increasing temperature to the next temperature level. Maximally 21% and 6% conversion was obtained with $Ca_3(PO_4)_2$ and $Ca_2P_2O_7$, respectively (Figure 5). Selectivity to acrylic acid was over the former catalyst maximally 51%, while for $Ca_2P_2O_7$ it was only 21% (Figure 4). These results are related to a low specific surface area of the latter catalyst as well as its high sodium amount.

When, however, temperature was increased and the experiments were started at 375 °C and continued up to 425 °C, much higher conversion (Figures 6 and 7) and the space-time yields of acrylic acid (Figure 8) were obtained. It can, however, be observed that the space time yield of acrylic acid was 3.4 fold higher with Ca_3PO_{42} than over $Ca_2(P_2O_7)$. It is also noteworthy that the space time yield for acrylic acid was increasing when increasing temperature from 375 °C to 400 °C, while at 425 °C only slightly higher maximum STY for acrylic acid was obtained. As a comparison, the space time yield for acrylic acid formation was calculated to be 16 µmol/(min· g_{cat}) over $Ca_3(PO_4)_2$ at 390 °C in Hong et al. (2011). This result indicates that the catalyst in the current work is even more active than previously reported (Hong et al. 2011).

Selectivity values to acrylic acid obtained for both $Ca_3(PO_4)_2$ and $Ca_2P_2O_7$ are presented in Figure 7d and Table 3. Selectivity to acrylic acid increased from the initial level of 46% to 58% at 78% conversion, whereafter it slightly deceased. Analogous results were obtained in Wang et al. (2014) in methyl lactate dehydration over K_2HPO_4-$Al_2(SO_4)_3$/MCM-41 catalyst in the temperature range of 320- 410 °C above which selectivity to acrylic acid decreased. In (Wang et al. 2014) such decrease was explained by a lower stability of the carboxylic group in the acrylic acid at a very high temperature. As a comparison to Hong et al. (2011) reporting methyl lactate (50 wt% in water) dehydration over $Ca_3(PO_4)_2$-$Ca_2(P_2O_7)$ in the temperature range of 350-400 °C it was observed that conversion increased from 30% to 95%, while acrylic acid selectivity decreased at the same time from 78% to 71%. In addition, selectivity to methyl acrylate and acetaldehyde increased from 3% to 6% and 13% to 16%.

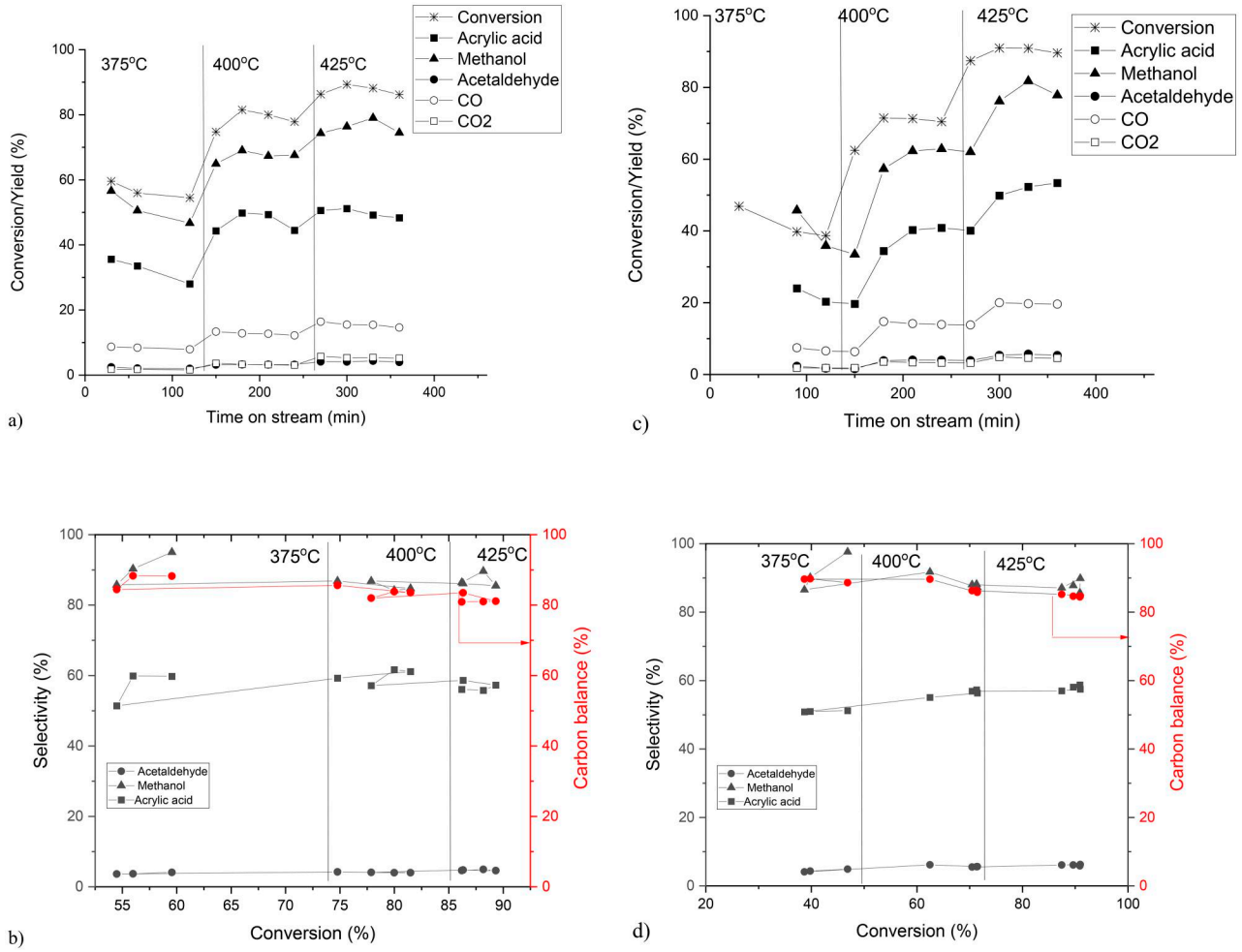

Figure 6. Methyl lactate transformation over $Ca_3(PO_4)_2$. (a) Conversion and concentration of components, (b) selectivity to different products and carbon balance as a function of conversion in, (c) and (d) are the corresponding graphs for $Ca_2(P_2O_7)$. Conditions: GHSV = 95280 h^{-1}, contact time 30 s. Notation: $Ca_3(PO_4)_2$ mass 150 mg, $Ca_2(P_2O_7)$ mass 500 mg, liquid flow 0.1 ml/min. The vertical lines correspond to changes in the temperature with the same catalyst.

When a mixture of $Ca_3(PO_4)_2$ and $Ca_2P_2O_7$ catalysts was used in methyl lactate transformations (Figure 9), the CO/CO_2 ratio decreased for $Ca_3(PO_4)_2$ with increasing conversion and temperature. For $Ca_2P_2O_7$ this ratio was nearly constant, while for the mixture of the two catalysts the CO/CO_2 ratio increasing initially up to 73% conversion, after which it remained nearly constant at the level of 9.8. These results showed clearly that $Ca_3(PO_4)_2$ with a higher acidity promoted decarboxylation, because the CO/CO_2 ratio decreased at 425 °C (Tables 3 and 4), while similar values were obtained for acrylic acid and methanol. At the same time, selectivity to acetaldehyde increased slightly. It should also be noted that selectivity to acetaldehyde should also be higher for $Ca_3(PO_4)_2$ based on its acidity, even if acetaldehyde selectivity can be somewhat uncertain because of its low boiling point.

Long term stability in isothermal dehydration of methyl lactate at 400 °C was also investigated for $Ca_3(PO_4)_2$ (Figure 10a).

The extent of catalyst deactivation, defined as a decrease of conversion with time was 0.02%/min. The carbon balance in the liquid phase increased with increasing time on stream from 79% to 88%, which could be also connected to a decrease of activity with time-on-stream related to carbon deposition on the catalyst surface. Selectivity to acrylic acid decreased only slightly from the maximum value of 62% at 62% conversion to 57% at 87% conversion (Figure 10b), while selectivity to acetaldehyde of ca. 5% was constant. The CO/CO_2 ratio decreased with

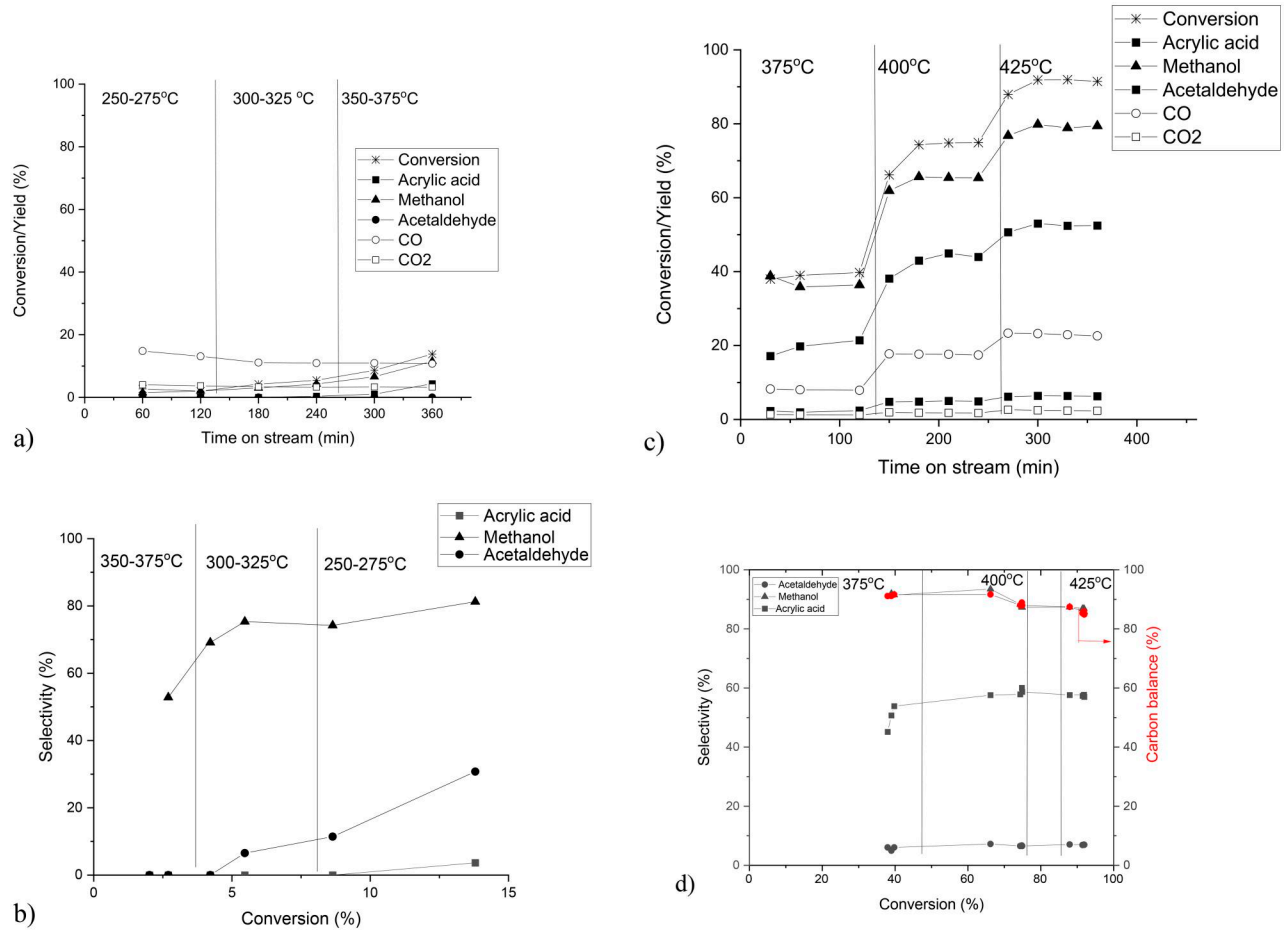

Figure 7. Methyl lactate transformation over a mixture of $Ca_3(PO_4)_2$ and $Ca_2(P_2O_7)$. (a) conversion and concentrations of components and (b) selectivity to different products and carbon balance as a function of conversion in in the temperature range of 275-375 °C, (c) and (d) the corresponding data in the temperature range of 375-425 °C. Conditions: GHSV = 95280 h^{-1}, contact time 30 s. Experimental conditions: catalyst mass 200 mg, liquid flow 0.1 ml/min. Carbon balance was not determined for the mixture at 250-375 °C.

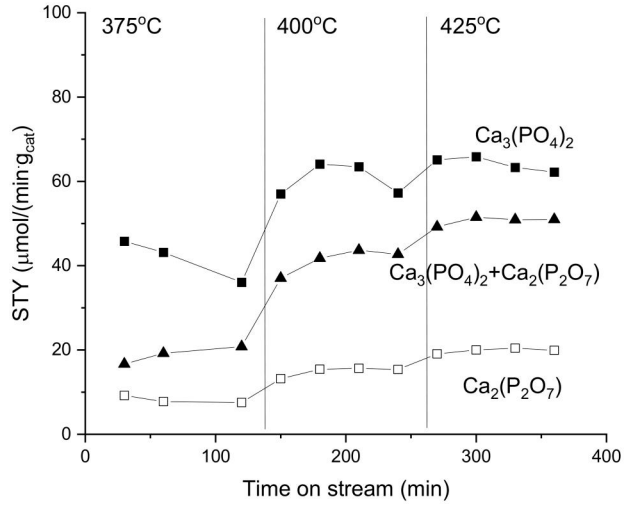

Figure 8. Space time yield for acrylic acid as a function of time on stream over $Ca_3(PO_4)_2$, $Ca_2(P_2O_7)$ and their mixture $Ca_3(PO_4)_2$-$Ca_2(P_2O_7)$ in the temperature range 375 °C to 425 °C.

increasing conversion from 4.0 to 2.6 (not depicted here) and methanol selectivity dropped from 92% to 87%, which is in line with the increased decarboxylation route.

Effect of gas hourly flow rate

Effect of the gas hourly space velocity varied with increasing TOS from 95280 h^{-1} to 31800 h^{-1} in methyl lactate transformations over $Ca_3(PO_4)_2$ at 400 °C (Figure 11).

The results demonstrated that conversion was initially decreasing with increasing TOS, however, after 120 min of TOS, conversion was not affected by the change in gas hourly space velocity because a high excess of argon molar flow in comparison to molar flow of methyl lactate was used. The extent

Table 3. Catalytic results from methyl lactate transformation to acrylic acid over $Ca_3(PO_4)_2$, $Ca_2P_2O_7$ and their mixture. Conditions: GHSV = 95280 h^{-1}, contact time 30 s at 85% conversion at 425 °C. Notation: CB is carbon balance.

Catalyst	mcat. (mg)	CB (%)	SAcrylic acid (%)	SAcetald (%)	SMeOH (%)	CO/CO2
$Ca_3(PO_4)_2$	150	87	57	4	87	1.6
$Ca_2P_2O_7$	500	86	57	6	87	4.2
$Ca_3(PO_4)_2$+$Ca_2P_2O_7$	200	87	57	7	86	9.2

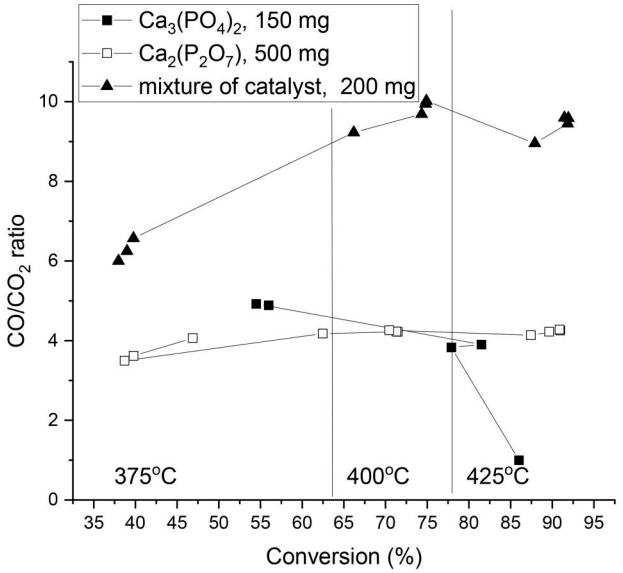

Figure 9. CO/CO_2 Ratio as a function of conversion for different catalysts. The catalyst amounts are $Ca(PO_4)_3$ 150 mg, $Ca_2(P_2O_7)$ 500 mg, and 200 mg for the mixture.

Table 4. Methyl lactate transformations at 400 °C over $Ca(PO_4)_2$ catalysts using neat and 80 wt% methyl lactate as a feedstock at 20% conversion.

Feed	$S_{acrylic\ acid}$ (%)	$S_{methyl\ acrylate}$ (%)	S_{MeOH} (%)	$S_{acetaldehyde}$ (%)	CO/CO_2
Neat methyl lactate	9	13	42	1	1.2
80 wt% methyl lactate	22	3.4	71	5	1.75

of catalyst deactivation was initially 0.13%/min, however, decreasing to the level of 0.02%/min for 63480 h^{-1} and 31800 h^{-1} gas space hourly velocities. Carbon balance in the liquid phase increased slightly from ca. 81% to ca. 88% with increasing TOS from 30 min to 360 min when conversion decreased from 87% to 64%, respectively. However, acetaldehyde selectivity increased with the lowest gas hourly space velocity. As a comparison analogously a lower carrier gas flow rate (smaller gas hourly space velocity) gave lower acrylic acid selectivity in methyl lactate transformations over modified $CaSO_4$ catalyst at 400 °C (Zhang et al. 2008). The gas phase analysis showed that CO/CO_2 ratio decreased with increasing conversion from 3.7 to 3.0.

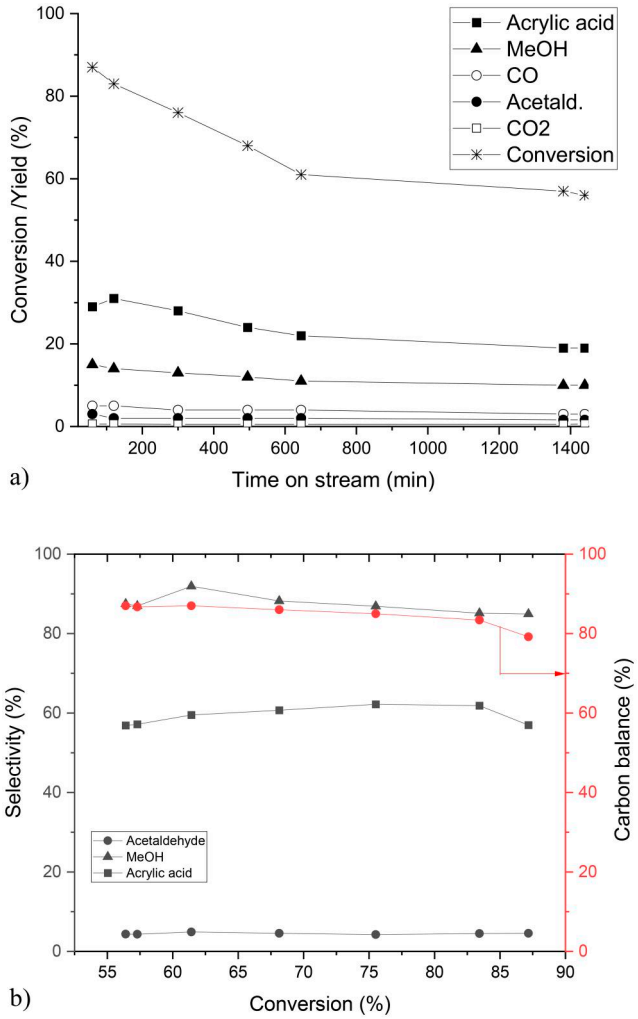

Figure 10. Methyl lactate transformation over $Ca_3(PO_4)_2$ at 400 °C: (a) conversion and yield as a function of time-on-stream, and (b) selectivity and carbon balance as a function of conversion. Conditions: GHSV = 95280 h^{-1}, contact time 30 s. Experimental conditions: catalyst mass 150 mg, liquid flow 0.1 ml/min.

Effect of liquid hourly space velocity

The effect of the liquid phase hourly space velocity, investigated by varying it in the range of 30-120 s (Figure 12), demonstrated that when conversion decreased at shorter residence times, selectivity remained quite constant pointing out on parallel reactions.

The carbon balance in the liquid phase increased from 83% with 30 s residence time to

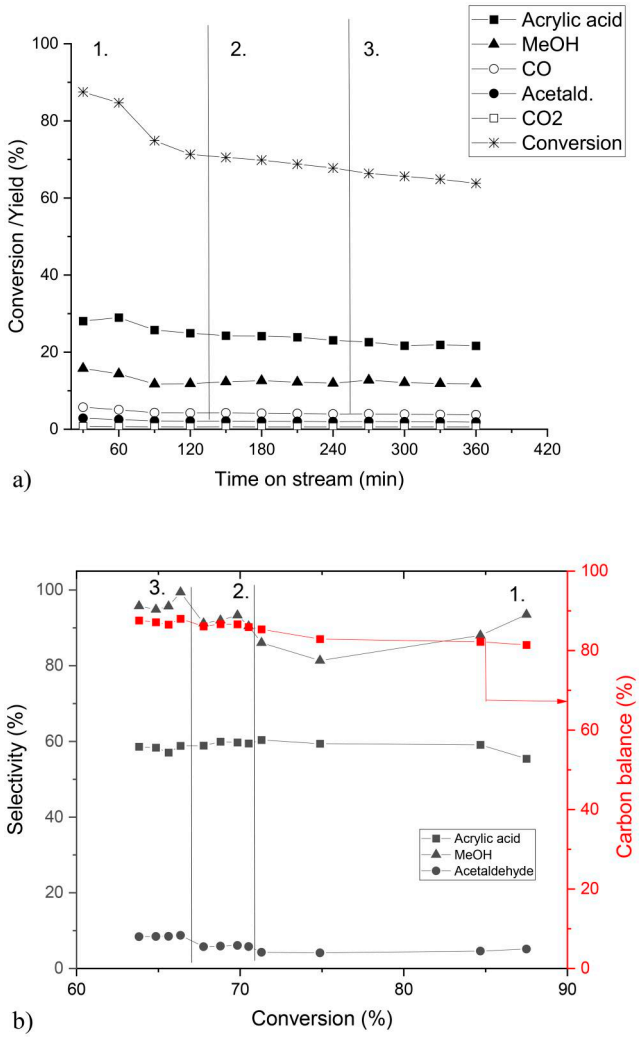

Figure 11. Methyl lactate transformation over $Ca_3(PO_4)_2$ at 400 °C, (a) conversion and yield vs time on stream, (b) selectivity and carbon balance as a function of conversion. Notation: Gas hourly space velocity (GHSV) 1. 95280 h^{-1}, 2. 63480 h^{-1} and 3. 31800 h^{-1}. Experimental conditions: catalyst mass 150 mg, liquid flow 0.1 ml/min.

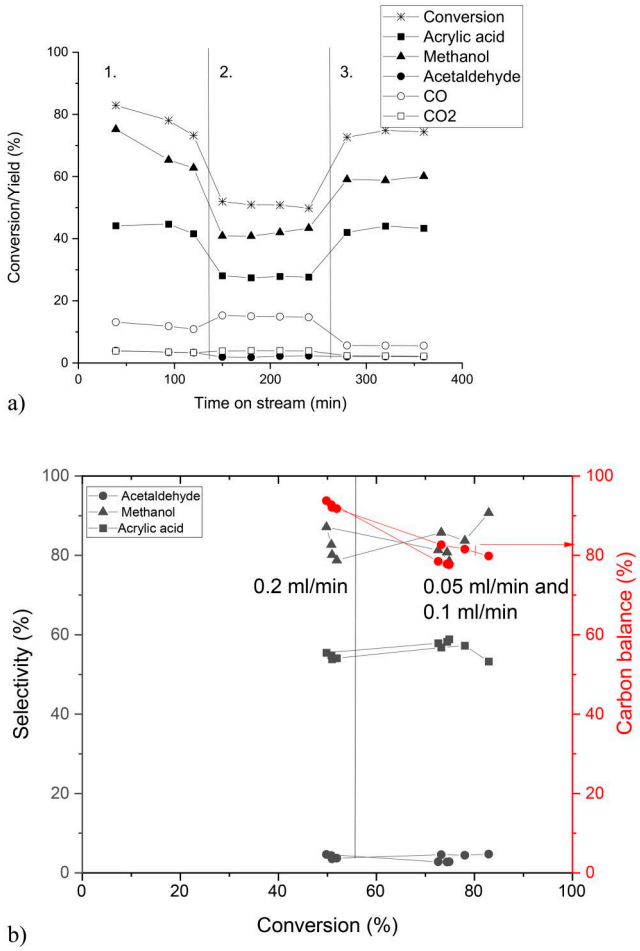

Figure 12. Methyl lactate transformation over $Ca_3(PO_4)_2$ at 400 °C using different liquid flow rates. (a) Conversion and concentrations of components, (b) selectivity and carbon balance as a function of conversion in GHSV = 95280 h^{-1}, liquid contact time 30, 60 and 120 s. Experimental conditions: catalyst mass 150 mg, liquid flow 0.05, 0.1 and 0.2 ml/min.

94% for 60 s residence time. Further increase to 120 s resulted in 78% carbon balance closure, which can be explained by more prominent formation of oligomers not visible in the GC analysis. The gas phase analysis revealed that CO/CO_2 ratio was the highest for the shortest liquid residence time of 30 s being 4.0, while for 60 s and 120 s it was 3.4 and 2.4, respectively.

Effect of initial methyl lactate concentration

When the initial concentration of methyl lactate in the feed was also varied in the range of 2-10 wt% no methyl acrylate was visible in the product mixture, while with neat and 80 wt% methyl lactate methyl acrylate was also present (see below). Initially the extent of catalyst deactivation was 0.098%/min when using 2 wt% methyl lactate in the feed. The deactivation rate increased by a factor 12 when increasing the initial methyl lactate concentration to 5 wt%. When additionally increasing the methyl lactate yield to 10 wt%, a further activity decline was rather minor.

The carbon balance in the liquid phase increased with increasing TOS after each adjustment of the liquid flow rate (Figure 13).

Selectivity to acrylic acid increased with increasing TOS after each change in the initial methyl lactate concentration. With the highest initial methyl lactate concentration only 53.5% selectivity to acrylic acid was obtained in comparison to ca. 58% at lower initial methyl lactate concentrations. A steady-state selectivity to acrylic acid was

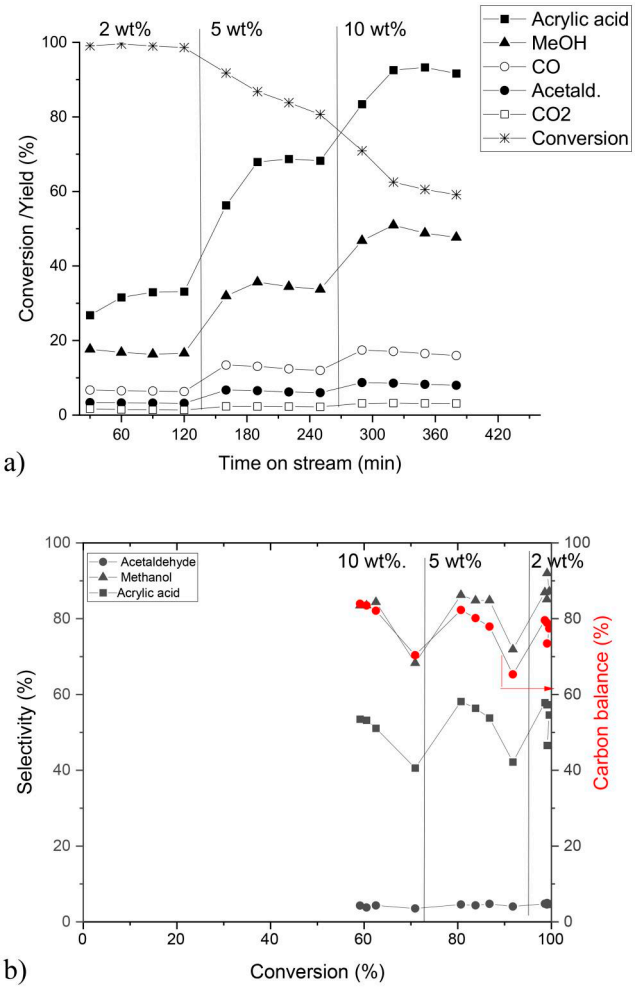

Figure 13. Methyl lactate transformation over $Ca_3(PO_4)_2$ at 400 °C using different initial concentrations of methyl lactate. Selectivity and the carbon balance as a function of conversion. Experimental conditions: catalyst mass 500 mg, liquid flow 0.1 ml/min.

not achieved with increasing TOS, while selectivity to acetaldehyde was constant.

The results using higher initial methyl lactate concentrations (neat and 80 wt% methyl lactate) are shown in Figures 14 and 15. Conversion decreased more rapidly with the neat methyl lactate as a feed (Figure 14).

The carbon balance and selectivity to different liquid phase products are depicted as a function of conversion using neat and 80% methyl lactate as a feed in Figure 15. Carbon balance increased from 73 to 100% with decreasing conversion from with neat methyl lactate as a feedstock and an analogous trend was observed for 80 wt% methyl lactate as a feed. The steady state rate for transforming methyl lactate, reached after 100-200 min of TOS and defined as moles of converted

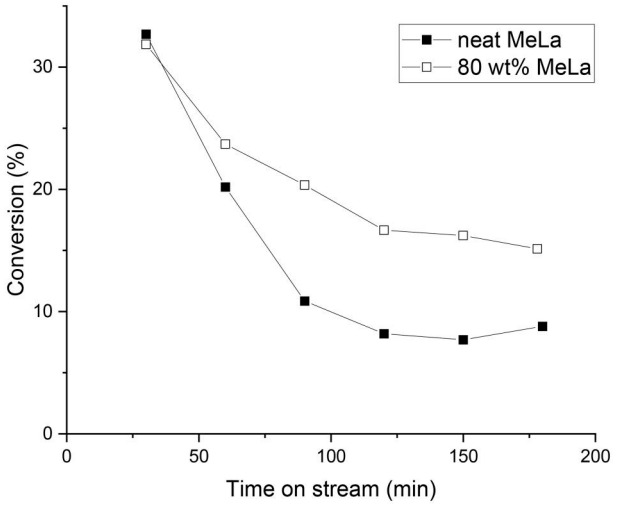

Figure 14. Conversion of methyl lactate (MeLa) as a function of TOS at 400 °C with and 80 wt% methyl lactate as a feed. Experimental conditions: catalyst mass 400 mg, liquid flow 0.1 ml/min.

methyl lactate per minute per catalyst mass, were 0.2 mmol/min/g_{cat} and 0.32 mmol/min/g_{cat} for neat and 80 wt% methyl lactate, respectively, over $Ca_2(PO_4)_2$ catalyst at 400 °C. The deactivation rate, defined as the decrease of conversion per time interval (%/min), with neat methyl lactate was 0.13%/min, while for 80 wt% methyl lactate the corresponding value was lower (0.09%/min) showing that a higher methyl lactate concentration increases catalyst deactivation (Figure 14) in qualitative agreement with (Zhang et al. 2008).

In methyl lactate transformation over $Ca_3(PO_4)_2$ selectivity to the sum of acrylic acid and methyl acrylate increased only slightly from 7% to 14% after which it started to decrease when using neat methyl lactate as a feed. However, in the presence of water the yield of acrylic acid was continuously increasing until 120 min TOS up to ca. 5% after which it remained nearly constant (Figure 14c). This result is also in accordance with (Zhang et al. 2008), when $CaSO_4$ was used as a promoter for $CuSO_4{\cdot}5H_2O{\cdot}Na_2HPO_4$. In (Zhang et al. 2008) the highest selectivity to the sum of acrylic acid and methyl acrylate was 80% with the initial methyl lactate concentration of 60% in the feed, while for the neat methyl lactate it was only 46%. The authors also stated (Zhang et al. 2008) that water could inhibit catalyst deactivation minimizing acrylate formation by promoting its hydrolysis.

When comparing selectivity of both liquid and gas phase products in methyl lactate transformation

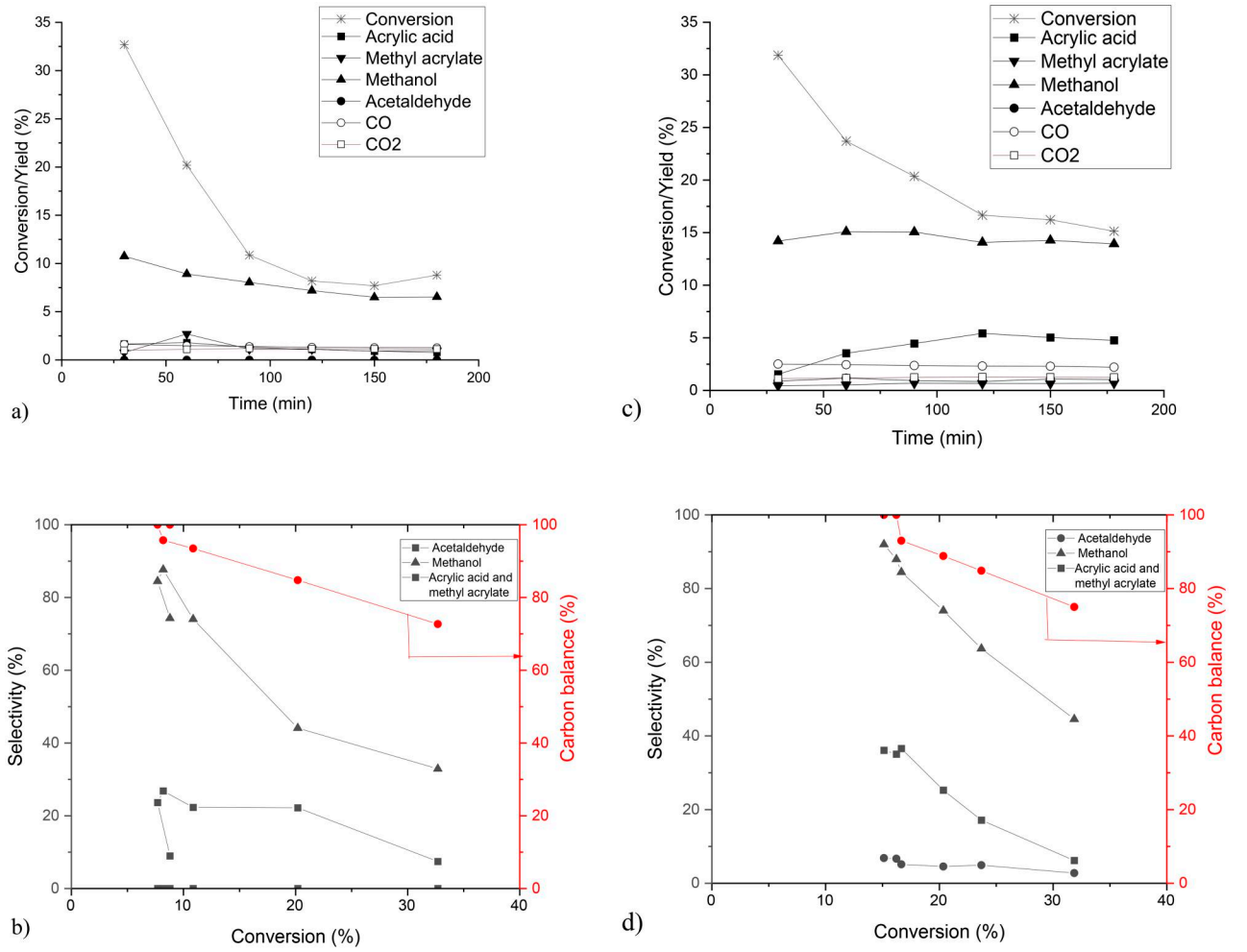

Figure 15. Methyl lactate transformation over $Ca_3(PO_4)_2$ at 400 °C using neat lactate. (a) Conversion and concentrations of components and (b) selectivity to different products and carbon balance as a function of conversion, (c) and (d) are the corresponding pictures for 80 wt% methyl lactate. Experimental conditions: catalyst mass 400 mg, liquid flow 0.1 ml/min.

over $Ca_3(PO_3)_2$ at 400 °C with neat and 80 wt% methyl lactate as a feedstock (Table 4), it can be seen that more methanol is formed in the presence of water, while selectivity to methyl acrylate was lower.

When the concentration of methyl acrylate is plotted as a function of the concentration of acrylic acid (Figure 16), it could be seen that with neat methyl lactate formation of acrylic acid was very slow after 30 min time on stream even decreasing after 60 min TOS, while methyl acrylate concentration remained constant after prolonged TOS. On the other hand, with 80% methyl lactate concentration in the feed, a much higher concentration of acrylic acid was obtained with prolonged time and the concentration of methyl acrylate increased only slightly with TOS, remaining nearly

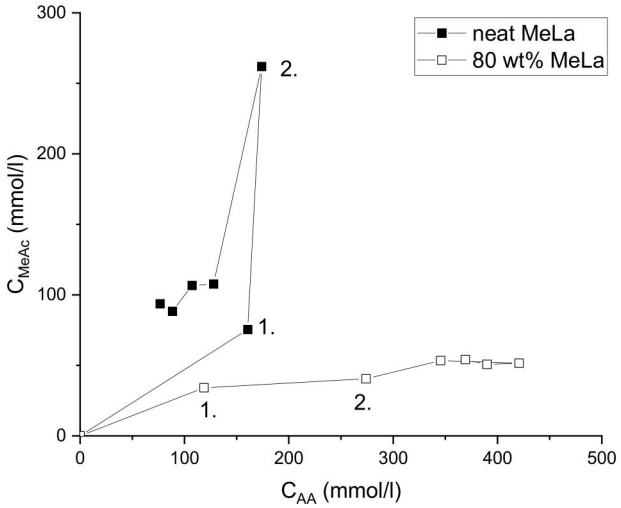

Figure 16. Concentration of methyl acrylate as a function of the concentration of acrylic acid in methyl lactate transformation using neat or 80 wt% methyl lactate as a feed at 400 °C for (1) 30 min TOS and (2) 60 min TOS.

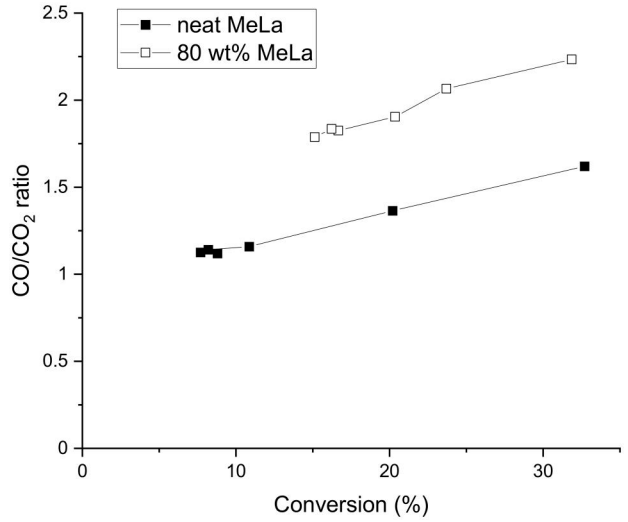

Figure 17. The CO/CO_2 ratio as a function of conversion in methyl lactate transformation with neat and 80 wt% methyl lactate as a feed at 400 °C with 400 mg of $Ca_3(PO_4)_2$.

constant after 90 min. This result indicates that water facilitated hydrolysis of methyl acrylate to a certain extent and concentration of acrylic acid exhibited a maximum at 120 min TOS, after which it declined by 12%. When acrylic acid concentration started to decrease, acetaldehyde concentration increased at the same time to ca. 21%.

The results from the gas phase analysis showed that the CO/CO_2 ratio decreased with decreasing conversion when TOS increased. Furthermore, this ratio was much higher when 80 wt% methyl lactate was used as a feed in comparison to neat methyl lactate (Figure 17), reflecting more prominent initial decarbonylation, while with increasing TOS and declining catalyst activity, enhanced decarboxylation was observed.

Reactor modeling

Quantification of the catalytic performance was done through reactor modeling applying the dynamic plug flow reactor model as follows:

$$\frac{d\ \dot{n}_i}{dt} = -w\frac{d\dot{n}_i}{dl} + \dot{V}m_{cat}r_i \tag{5}$$

with the following boundary values

$$\left(\frac{d\ \dot{n}_i}{dt}\right)_{l=0} = (\dot{n}_{0i} - \dot{n}_i) \tag{6}$$

$$\left(\frac{d\ \dot{n}_i}{dt}\right)_{l=L} = \frac{d\dot{n}_i}{dl} \tag{7}$$

where $\dot{n}_{0i}$ and $\dot{n}_i$ denote the initial molar flow and molar flow at time t, m_{cat} is the catalyst mass, l is the reactor length, w is the gas velocity, $\dot{V}$ is the volumetric liquid flow.

The generation rates for the reactant as well as for methanol, acrylic acid and acetaldehyde were defined as:

$$\text{Methyl lactate} \rightarrow \text{Acetaldehyde (reaction 1)} \tag{8}$$

$$\text{Methyl lactate} \rightarrow \text{Methanol (reaction 2)} \tag{9}$$

$$\text{Methyl lactate} \rightarrow \text{Acrylic acid (reaction 3)} \tag{10}$$

The reaction rates for reactions 1-3 were assumed to follow the first order kinetics in methyl lactate

$$r_1 = k_1\frac{\dot{n}_{ML}}{\dot{V}} \tag{11}$$

$$r_2 = k_2\frac{\dot{n}_{ML}}{\dot{V}} \tag{12}$$

$$r_3 = k_3\frac{\dot{n}_{ML}}{\dot{V}} \tag{13}$$

In Equations (11–13) k_i denotes rate constants of the corresponding reactions.

Numerically Equation (5) was converted to ordinary differential equations (ODE:s) by using the finite difference approximation, and the obtained ODE:s were then solved by the backward difference method. For estimation of the unknown parameters Simplex and/or the Levenberg-Marquardt method was used. The numerical tools are built into the software for modeling and optimization ModEst (Haario 2001).

The results from kinetic modeling illustrated in Figure 18a–c and Table 5 confirm a good fit of the experimental data which is also reflected by high values of the degree of explanation being 97.15% for $Ca_3(PO_4)_2$, 95.40% $Ca_2P_2O_7$ and 94.53% for $Ca_3(PO_4)_2$ and $Ca_2P_2O_7$, respectively. In addition, simulated concentration values for different components are presented in Figure 18d for the methyl lactate transformation over a mixture of $Ca_3(PO_4)_2$ + $Ca_2P_2O_7$ when using the parameters obtained separately from $Ca_3(PO_4)_2$ and $Ca_2P_2O_7$.

The rate constants for formation of acrylic acid were always ca. two fold those of acetaldehyde, while the rate constant for methanol formation was the smallest one. On the other hand, the activation energy for formation of acetaldehyde and acrylic acid was approximately the same for $Ca_3(PO_4)_2$,

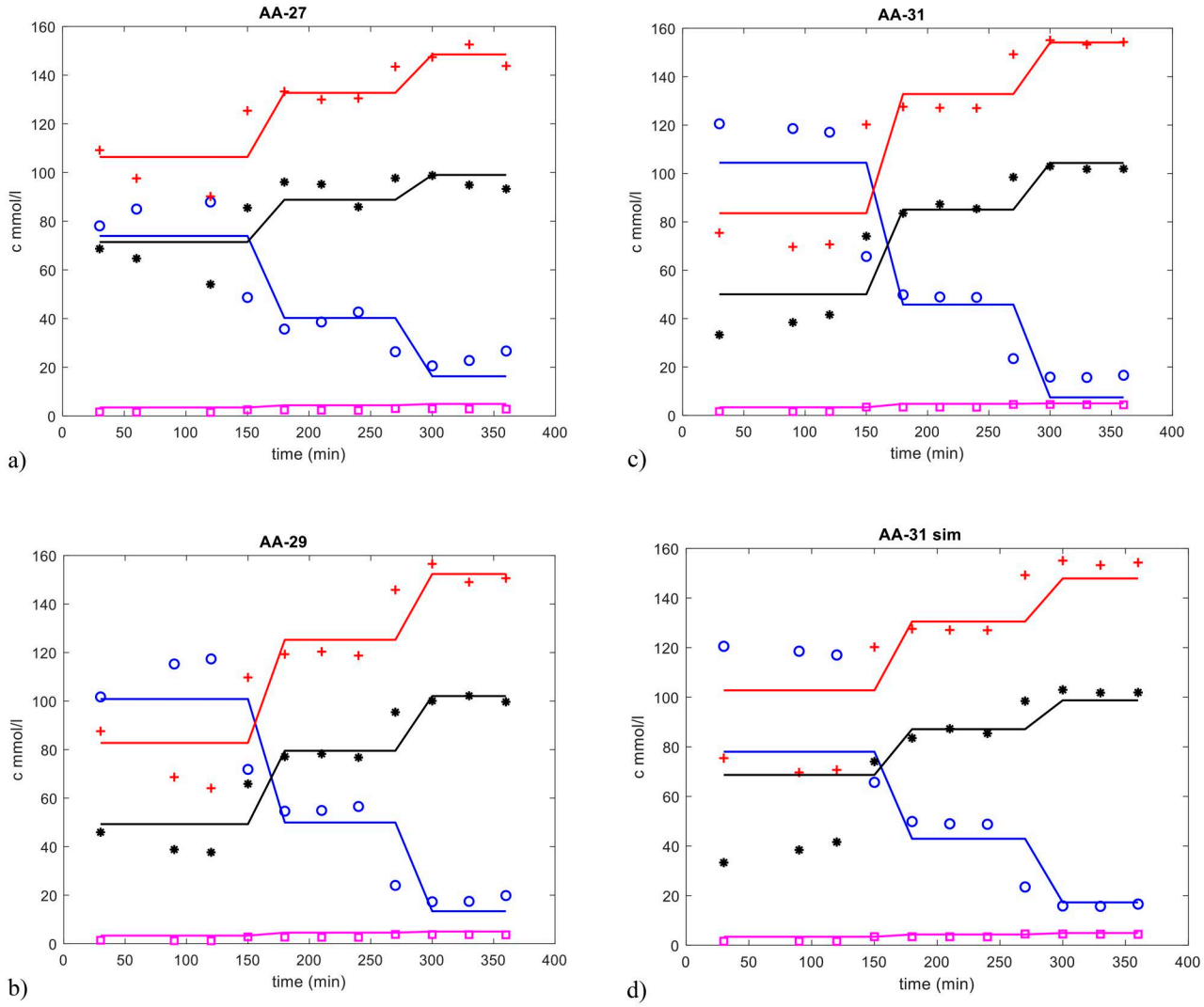

Figure 18. Concentration of methyl lactate (blue, o), methanol (red, +), acrylic acid (black,*) and acetaldehyde (purple, o).

Table 5. Parameter values and relative standard errors obtained in methyl lactate transformation over different catalysts.

	$Ca_3(PO_4)_2$		$Ca_2P_2O_7$		$Ca_3(PO_4)_2 + Ca_2(P_2O_7)$	
Parameter	Parameter value	Relative standard error (%)	Parameter value	Relative standard error (%)	Parameter value	Relative standard error (%)
k1 (min^{-1})	10.1	9.1	0.87	11.4	5.89	13.1
k2 (min^{-1})	4.4	22.9	0.32	34.3	1.66	56.8
k3 (min^{-1})	20.5	4.4	1.52	6.0	10.7	7.2
EA1 (kJ/mol)	74.1	23.7	93.2	23.5	107	23.5
EA2 (kJ/mol)	111	37.2	148	41.7	228	40.8
EA5 (kJ/mol)	72.4	11.5	117	10.6	132	11.7

while for $Ca_2P_2O_7$ the activation energy for acetaldehyde formation was lower than the one for acrylic acid.

As a comparison, activation energies for reactions 1-4 in Scheme 1 were determined for methyl lactate dehydration over $CaSO_4$ catalyst promoted by KH_2PO_4, Na_2HPO_4 and $CuSO_4$. For formation of methyl acrylate (reaction 1) the activation energy was 38.1 kJ/mol in good agreement with the current work, while for formation of acrylic acid (reaction 2) and acetaldehyde (reaction 3 and 4) the corresponding activation energies were 64.1 kJ/mol and 65.2 kJ/mol, respectively (Zhang et al. 2008).

Conclusions

Transformation of methyl lactate to acrylic acid was investigated using $Ca_3(PO_4)_2$, $Ca_2P_2O_7$ and

their mixture as catalysts in the temperature range of 250 – 425 °C using 2 wt% methyl lactate as a feed. These catalysts prepared in house did not exhibit any measurable basicity, acidity, measured by NH_3-TPD, were 485 µmol/g for the $Ca_3(PO_4)_2$ and 43 µmol/g for the $Ca_2P_2O_7$ catalysts. The specific surface area of $Ca_3(PO_4)_2$ was 16 m^2/g, while for $Ca_2P_2O_7$ it was less than 1 m^2/g. The catalytic results showed that only above 375 °C sufficient conversions were obtained, being 89% for $Ca_3(PO_4)_2$ and 90% for $Ca_2P_2O_7$, respectively at 425 °C with gas hourly space velocity of 95280 h^{-1}. The maximum space time yield for acrylic acid was 62 mmol/(min· g_{cat}) for $Ca_3(PO_4)_2$, while for $Ca_2P_2O_7$ it was 3.4 fold lower, which can be explained by a low surface area of the latter catalyst. In addition, Ca/P ratio in the spent catalysts decreased 17% for $Ca_2P_2O_7$, while the corresponding decrease for $Ca_3(PO_4)_2$ was only 5%. Kinetic constants and activation energies were determined by kinetic modeling resulting in the activation energy for formation of acrylic acid and acetaldehyde of 64.1 kJ/mol and 65.2 kJ/mol, respectively.

The effect of other parameters, such as the liquid and gas flow rates and initial methyl lactate concentration in the feed were also investigated. The results showed that selectivity remained constant when changing the residence time, pointing out on parallel reactions for formation of acrylic acid and acetaldehyde. The effect of gas hourly space velocity on selectivity was inferior. Conversion of methyl lactate decreased with increasing initial methyl lactate concentration and at the same time selectivity to acrylic acid and methyl acrylate decreased. Furthermore, when using 80 wt% methyl lactate in the feed, the initial decarbonylation was more prominent than in the case of neat methyl lactate as a feedstock. Catalytic activity, however, declined with increasing time-on-stream and at the same time decarbonylation reaction was enhanced. Long-term stability tests with $Ca_3(PO_4)_2$ showed that after initial deactivation during 11 h time-on-stream the activity dropped only slightly. At the same time, selectivity to acrylic acid dropped from 62% only to 57%.

Disclosure statement

Co-authors do not have any relevant financial or non-financial competing interests.

References

Ardanova LI, Get'man EI, Loboda SN, Prisedsky VV, Tkachenko TV, Marchenko VI, Antonovich VP, Chivireva NA, Chebishev KA, Lyashenko AS. 2010. Isomorphous substitutions of rare earth elements for calcium in synthetic hydroxyapatites. Inorg Chem. 49(22): 10687–10693., doi:10.1021/ic1015127.

Ben Amara M, Vlasse M, Le Flem G, Hagenmuller P. 1983. Structure of the low-temperature variety of calcium sodium orthophosphate, NaCaPO4. Acta Crystallogr C Cryst Struct Commun. 3939(11):1483–1485. doi:10.1107/S0108270183008963.

Bennazha J, Boukhari A, Holt EM. 1999. Synthesis and crystal structure of Na2CaP2O7. Solid State Sci. 1(6):373–380. doi:10.1016/S1293-2558(00)80091-6.

Blanco E, Delichere P, Millet JMM, Loridant S. 2014. Gas phase dehydration of lactic acid to acrylic acid over alkaline-earth phosphates catalysts. Catal. Today, Acid-Base Catalysis Advanced Sciences and Spreading Applications to Solutions of Environmental, Resources and Energy Issues: ABC-7, 7th International Symposium on Acid-Base Catalysis, Tokyo, May 12-15, 2013 226, 185–191. doi:10.1016/j.cattod.2013.09.059.

Boudin S, Grandin A, Borel MM, Leclaire A, Raveau B. 1993. Redetermination of the β-Ca2P2O7 structure. Acta Crystallogr C Cryst Struct Commun. 49(12):2062–2064. doi:10.1107/S0108270193005608.

Burk MJ, Pharkya P, Dien SJV, Burgard AP, Schilling CH. 2011. Methods for the synthesis of acrylic acid and derivatives from fumaric acid. EP2348008A1.

Craciun L, Benn GP, Dewing J, Schriver GW, Peer WJ, Siebenhaar B, Siegrist U. 2009. Preparation of acrylic acid derivatives from α- or β-hydroxy carboxylic acids. US7538247B2.

Datta R, Henry M. 2006. Lactic acid: recent advances in products, processes and technologies—a review. J Chem Tech Biotech. 81(7):1119–1129. doi:10.1002/jctb.1486.

Dhiman N, Reddy Yenumala S, Agrawal D, Pandey A, Porwal J, Sarkar B. 2023. Production of acrylic acid from Bio-Derived lactic acid over a Defect-Rich molybdenum phosphosulfide catalyst. Chem Eng J. 466:143240. doi:10.1016/j.cej.2023.143240.

Ghantani VC, Dongare MK, Umbarkar SB. 2014. Nonstoichiometric calcium pyrophosphate: a highly efficient and selective catalyst for dehydration of lactic acid to acrylic acid. RSC Adv. 4(63):33319–33326. doi:10.1039/C4RA06429A.

Ghantani VC, Lomate ST, Dongare MK, Umbarkar SB. 2013. Catalytic dehydration of lactic acid to acrylic acid using calcium hydroxyapatite catalysts. Green Chem. 15(5):1211–1217. doi:10.1039/c3gc40144h.

Haario H. 2001. ModEst users guide. Helsinki: ProfMath Oy.

Holmen RE. 1958. Production of acrylates by catalytic dehydration of lactic acid and alkyl lactates. US2859240A.

Hong JH, Lee J-M, Kim H, Hwang YK, Chang J-S, Halligudi SB, Han Y-H. 2011. Efficient and selective conversion of methyl lactate to acrylic acid using Ca3(PO4)2–Ca2(P2O7) composite catalysts. Appl. Catal. Gen. 396(1-2): 194–200. doi:10.1016/j.apcata.2011.02.015.

Jiang X, Meng X, Xian M. 2009. Biosynthetic pathways for 3-hydroxypropionic acid production. Appl Microbiol Biotechnol. 82(6):995–1003. doi:10.1007/s00253-009-1898-7.

Lari GM, Puértolas B, Frei MS, Mondelli C, Pérez-Ramírez J. 2016. Hierarchical NaY zeolites for lactic acid dehydration to acrylic acid. ChemCatChem. 8(8):1507–1514. doi:10.1002/cctc.201600102.

Lee J-M, Hwang D-W, Hwang YK, Halligudi SB, Chang J-S, Han Y-H. 2010. Efficient dehydration of methyl lactate to acrylic acid using Ca3(PO4)2–SiO2 catalyst. Catal Commun. 11(15):1176–1180. doi:10.1016/j.catcom.2010.06.013.

Li C, Wang B, Zhu Q, Tan T. 2014. Efficient catalytic dehydration of methyl lactate to acrylic acid using sulphate and phosphate modified MCM-41 catalysts. Appl Catal Gen. 487:219–225. doi:10.1016/j.apcata.2014.09.011.

Liu Z-H, Yan B, Liang Y, Xu B-Q. 2020. Comparative study of gas-phase "dehydration" of alkyl lactates and lactic acid for acrylic acid production over hydroxyapatite catalysts. Mol. Catal. 494:111098. doi:10.1016/j.mcat.2020.111098.

Mäki-Arvela P, Aho A, Murzin D. 2020. Heterogeneous catalytic synthesis of methyl lactate and lactic acid from sugars and their derivatives. ChemSusChem. 13(18): 4833–4855. doi:10.1002/cssc.202001223.

Murphy BM, Letterio MP, Xu B. 2017. Catalyst deactivation in pyridine-assisted selective dehydration of methyl lactate on NaY. ACS Catal. 7(3):1912–1930. doi:10.1021/acscatal.6b03166.

Murphy BM, Letterio MP, Xu B. 2016a. Catalytic dehydration of methyl lactate: reaction mechanism and selectivity control. J Catal. 339:21–30. doi:10.1016/j.jcat.2016.03.026.

Murphy BM, Letterio MP, Xu B. 2016b. Selectivity control in the catalytic dehydration of methyl lactate: the effect of pyridine. ACS Catal. 6(8):5117–5131. doi:10.1021/acscatal.6b00723.

Murphy BM, Mou T, Wang B, Xu B. 2018. The effect of cofed species on the kinetics of catalytic methyl lactate dehydration on NaY. ACS Catal. 8(10):9066–9078. doi:10.1021/acscatal.8b02125.

Näfe G, López-Martínez M-A, Dyballa M, Hunger M, Traa Y, Hirth T, Klemm E. 2015. Deactivation behavior of alkali-metal zeolites in the dehydration of lactic acid to acrylic acid. J. Catal. 329:413–424. doi:10.1016/j.jcat.2015.05.017.

Nekkala N, Balla P, Ginjupalli SR, Seelam PK, S.k H, Ponnala B, Komandur VRC. 2022. Lanthanum phosphate: an efficient catalyst for acrylic acid production through lactic acid dehydration. Biomass Conv Bioref. 12(8):3535–3546. doi:10.1007/s13399-020-01148-4.

Peng J, Li X, Tang C, Bai W. 2014. Barium sulphate catalyzed dehydration of lactic acid to acrylic acid. Green Chem. 16(1):108–111. doi:10.1039/C3GC42028K.

Rodrigues JL. 2022. Heterologous production of acrylic acid: current challenges and perspectives. SynBio. 1(1):3–32. doi:10.3390/synbio1010002.

Shi HF, Hu YC, Wang Y, Huang H. 2007. KNaY-zeolite catalyzed dehydration of methyl lactate. Chin Chem Lett. 18(4):476–478. doi:10.1016/j.cclet.2007.01.043.

Sobuś N, Czekaj I. 2022. Lactic acid conversion into acrylic acid and other products over natural and synthetic zeolite catalysts: theoretical and experimental studies. Catal Today. 387:172–185. doi:10.1016/j.cattod.2021.10.021.

Sun P, Yu D, Fu K, Gu M, Wang Y, Huang H, Ying H. 2009. Potassium modified NaY: a selective and durable catalyst for dehydration of lactic acid to acrylic acid. Catal Commun. 10(9):1345–1349. doi:10.1016/j.catcom.2009.02.019.

Sun P, Yu D, Tang Z, Li H, Huang H. 2010. NaY zeolites catalyze dehydration of lactic acid to acrylic acid: studies on the effects of anions in potassium salts. Ind Eng Chem Res. 49(19):9082–9087. doi:10.1021/ie101093x.

Talebian-Kiakalaieh A, Amin NAS, Hezaveh H. 2014. Glycerol for renewable acrolein production by catalytic dehydration. Renew Sustain Energy Rev. 40:28–59. doi:10.1016/j.rser.2014.07.168.

Tam MS, Gunter GC, Craciun R, Miller DJ, Jackson JE. 1997. Reaction and spectroscopic studies of sodium salt catalysts for lactic acid conversion. Ind Eng Chem Res. 36(9):3505–3512. doi:10.1021/ie970014m.

Tang C, Peng J, Fan G, Li X, Pu X, Bai W. 2014a. Catalytic dehydration of lactic acid to acrylic acid over dibarium pyrophosphate. Catal Commun. 43:231–234. doi:10.1016/j.catcom.2013.10.009.

Tang C, Peng J, Li X, Zhai Z, Jiang N, Bai W, Gao H, Liao Y. 2014b. Strontium pyrophosphate modified by phosphoric acid for the dehydration of lactic acid to acrylic acid. RSC Adv. 4(55):28875–28882. doi:10.1039/C4RA03398A.

Tichý J. 1997. Oxidation of acrolein to acrylic acid over vanadium-molybdenum oxide catalysts. Appl Catal Gen. 157(1-2):363–385. doi:10.1016/S0926-860X(97)00025-2.

Walkup PC, Rohrmann CA, Hallen RT, Eakin DE. 1993. Production of esters of lactic acid, esters of acrylic acid, lactic acid, and acrylic acid. US5252473A.

Wang B, Li C, Zhu Q, Tan T. 2014. The effect of K2HPO4 and Al2(SO4)3 modified MCM-41 on the dehydration of methyl lactate to acrylic acid. RSC Adv. 4(86):45679–45686. doi:10.1039/C4RA08738K.

Wang H, Yu D, Sun P, Yan J, Wang Y, Huang H. 2008. Rare earth metal modified NaY: structure and catalytic performance for lactic acid dehydration to acrylic acid. Catal Commun. 9(9):1799–1803. doi:10.1016/j.catcom.2008.01.023.

Yan B, Liu Z-H, Liang Y, Xu B-Q. 2020. Acrylic acid production by gas-phase dehydration of lactic acid over K+-exchanged ZSM-5: reaction variable effects, kinetics, and new evidence for cooperative acid–base bifunctional catalysis. Ind Eng Chem Res. 59(39):17417–17428. doi:10.1021/acs.iecr.0c02148.

Yan B, Tao L-Z, Liang Y, Xu B-Q. 2014a. Sustainable production of acrylic acid: catalytic performance of hydroxyapatites

for gas-phase dehydration of lactic acid. ACS Catal. 4(6): 1931–1943. doi:10.1021/cs500388x.

Yan B, Tao L-Z, Liang Y, Xu B-Q. 2014b. Sustainable production of acrylic acid: alkali-ion exchanged Beta zeolite for gas-phase dehydration of lactic acid. ChemSusChem. 7(6):1568–1578. doi:10.1002/cssc.201400134.

Yan J, Yu D, Sun P, Huang H. 2011. Alkaline earth metal modified NaY for lactic acid dehydration to acrylic acid: effect of basic sites on the catalytic performance. Chin J Catal. 32(3-4):405–411. doi:10.1016/S1872-2067(10)60188-X.

Yuan C, Liu H, Zhang Z, Lu H, Zhu Q, Chen Y. 2015. Alkali-metal-modified ZSM-5 zeolites for improvement of catalytic dehydration of lactic acid to acrylic acid. Chin J Catal. 36(11):1861–1866. doi:10.1016/S1872-2067(15)60970-6.

Zhang J, Lin J, Xu X, Cen P. 2008. Evaluation of catalysts and optimization of reaction conditions for the dehydration of methyl lactate to acrylates. Chin J Chem Eng. 16(2):263–269. doi:10.1016/S1004-9541(08)60073-7.

Zhang J, Zhao Y, Feng X, Pan M, Zhao J, Ji W, Au C-T. 2014. Na2HPO4-modified NaY nanocrystallites: efficient catalyst for acrylic acid production through lactic acid dehydration. Catal Sci Technol. 4(5):1376–1385. doi:10.1039/C3CY00935A.

Zhang J, Zhao Y, Pan M, Feng X, Ji W, Au C-T. 2011. Efficient acrylic acid production through bio lactic acid dehydration over NaY zeolite modified by alkali phosphates. ACS Catal. 1(1):32–41. doi:10.1021/cs100047p.

Zhang X, Lin L, Zhang T, Liu H, Zhang X. 2016. Catalytic dehydration of lactic acid to acrylic acid over modified ZSM-5 catalysts. Chem Eng J. 284:934–941. doi:10.1016/j.cej.2015.09.039.

Zhang Z, Qu Y, Wang S, Wang J. 2009. Catalytic performance and characterization of silica supported sodium phosphates for the dehydration of methyl lactate to methyl scrylate and acrylic acid. Ind Eng Chem Res. 48(20):9083–9089. doi:10.1021/ie900065a.